07,11,12,13

Kinetics of polymorphic transformations of tricosane n-$C_{23}H_{48}$ upon heating

© S.A. Gureva[1], A.K. Borisov[1], V.A. Marikhin[1], M.V. Baidakova[1], E.S. Kulikova[2], P.V. Dorovatovskii[2]

[1] Ioffe Institute, St. Petersburg, Russia
[2] National Research Center „Kurchatov Institute", Moscow, Russia

E-mail: swet.gurjewa@gmail.com

Received April 20, 2025
Revised April 30, 2025
Accepted May 1, 2025

The polymorphic transformations of tricosane n-$C_{23}H_{48}$ upon heating were studied using synchrotron X-ray diffractometry and differential scanning calorimetry. The kinetics of the development of a sequence of solid-solid phase transitions was revealed. It was shown that the initial orthorhombic subcells of tricosane are gradually transformed into hexagonal ones, which is determined by the weakening van der Waals interaction between individual molecules and the occurrence of discrete rotation of molecules around their principal axes in the lamellae during thermal expansion of crystals. These transformations occur through the formation of a number of intermediate rotator phases (R_V, R_I, R_{II}). It was found that the phase transitions: ordered crystal $\rightarrow R_V$ and $R_I \rightarrow R_{II}$ are diffuse first-order phase transitions and develop according to a heterogeneous mechanism, and the phase transition $R_V \Rightarrow R_I$ refers to second-order transitions. The parameters of unit cells and their temperature changes in each of the observed polymorphic modifications of tricosane were determined.

Keywords: phase transitions, X-ray diffractometry, polymorphic transformations of tricosane.

DOI: 10.61011/PSS.2025.04.61273.99-25

1. Introduction

The study of temperature polymorphism of long-chain n-alkanes has remained a hot topic in polymer physics for many years [1–7] due to the lack of consensus on the mechanism of structural rearrangements during the transition from the solid state to the melt and vice versa. Most homologues of n-alkanes C_nH_{2n+2} with the number of carbon atoms in the chain $9 \leq n \leq 60$ show the occurrence of one, and often a number of intermediate phases arising from heating/cooling processes. Some of these intermediate phases have been called rotator phases, R) [8] because they are characterized by the presence of positional order in the absence of long-range orientational order. Rotator-crystalline R phases are intermediate between the fully ordered crystalline state and the isotropic liquid in long-chain n-alkanes. Their main difference from purely crystalline phases is the presence of discrete rotation of molecules around their axes, and each of the rotator phases is characterized by a certain number of equally probable orientations of molecules in lattice cells.

It is important to note that n-alkanes belong to the class of long-chain molecular crystals (LCMCs), the crystallization of which forms a multilevel supramolecular organization consisting of stacks of specific lamellar nanocrystals of the type „extended chain crystals" [9]. The thicknesses of the lamellae are comparable to the molecule length (units of nm) of the homologue in question; the transverse dimensions of the lamellae vary from units of μm to units of mm depending on crystallization conditions. The crystal core of the lamella is three-dimensionally packed methylene sequences with Van der Waals forces acting between them. The lamellar surface is formed of terminal methyl groups which, through Van der Waals interactions, form the contact of neighboring lamellae in stacks —so-called interlamellar layers.

Two types of crystal cells are considered in n-alkane crystals [9]: the main cell, which characterizes the way lamellae are stacked relative to each other in stacks, and the subcell, which describes the nature of the stacking of methylene trans-sequences in the crystalline cores of individual lamellae. The symmetry of individual n-alkane molecules (trans or cis-form) changes depending on the even/odd value of the number of carbon atoms in the chain (so called „parity effect"), and, this results in the change of the character of the arrangement of regular trans-zigzags in the crystal cores of nanolamellae relative to the base planes from the terminal methyl CH_3 groups. Thus, the structure of the ordered crystal phase of the n-alkanes homologue is determined by the trans- or cis-symmetry of the molecule and is characterized by either a vertical arrangement of chains in lamellae for odd homologues (orthorhombic main cell) or an inclined arrangement of chains (monoclinic/triclinic main cell) for even homologues. Symmetries of the main cell and subcell may differ.

As noted earlier, as temperature increases, polymorphic transformations are characteristic of n-alkanes, in particular, the appearance of rotator R phases in which a discrete rotation of molecules around their principal axes takes place within the crystal cores of nanolamellae throughout the crystal volume. Five different R phases of n-alkanes are currently distinguished depending on chain lengths and initial crystal symmetry [2,3], differing in the types of crystal core cells and subcells. Some studies of R phases have been described in Ref. [10–14] for homologues with chain lengths $11 \leq n \leq 34$. N-alkanes with $n < 27$ carbon atoms are characterized by the appearance of three rotator phases during heating: R_V, R_I and R_{II}. Phases R_V and R_I have orthorhombic subcells, while the main cells in the R_I phase are considered to be face-centered orthorhombic, whereas the molecules in phase R_V are arranged at some angle to form monoclinic main cells. Both phases are characterized by a double-layer sequence of ABAB-type lamellae stacking. The high-temperature phase R_{II} is characterized by vertically arranged molecules in lamellae with rhombohedral main cells and hexagonal subcells, with the lamellar stacking becoming an ABCABC-type triple-layer. The homologues of n-alkanes with greater values of n are characterized by the little-studied rotator phases R_{III} and R_{IV} [14]. The R_{III} phase is characterized by a triclinic main lattice cell, and R_{IV} phase is characterized by a monoclinic main lattice cell, with both cases treating the subcells as pseudohexagonal and the mutual stacking of the lamellae considered to be single-layer type AA.

The R phase is characterized by the fact that the crystal cores of the nanolamellae retain long-range order in the arrangement of the centers of macromolecules relative to each other (distance ordering), but the strict arrangement of the planes of the methylene trans-sequences (orientational disordering) is disrupted due to the rotation of the molecules. Moreover, the transition from one R phase to another during heating is associated with an increasing number of possible equiprobable orientations of the molecules in the subcells. Thus, the hexagonal phase (R_{II}) is said to exhibit complete orientational disordering of trans-zigzag planes in subcells.

The nature of the factors responsible for the temperature polymorphism of n-alkanes still remains unexplored. It can be hypothesized that the increasing number of defective molecules above some limiting concentration upon heating induces the emergence of a different molecular symmetry (similar to the differences induced by trans- and cis-symmetries), leading to the emergence of new rotator-crystalline structures. For this reason, there is a need for additional studies to elucidate the kinetics of structural rearrangements of long-chain n-alkanes. This work is devoted to the study of phase transformations in the odd n-alkane tricosane n-$C_{23}H_{48}$.

In future, the short notation for the homologues of n-alkanes — Cn will be used, i.e., we will define tricosane as C23, etc.

2. Polymorphic modifications of tricosane n-$C_{23}H_{48}$

The lowest temperature modification of monodisperse odd n-alkanes (n from 9 to 45) is consistent with the orthorhombic structure determined by Smith [15] for tricosane n-$C_{23}H_{48}$ and having space group $Pbcm$ (57).

According to the literature [13,16–18], the transition of the original orthorhombic phase 38 °C to a new high-temperature orthorhombic phase O_{dci} with space group $Pbnm$ (62) occurs in C23 as the temperature increases, near 38 °C. The lower index i (French *impair*) emphasizes the attribution of the phase to odd n-alkanes. The index dci stands for „defauts de conformation dans les alcanes impairs“, which means „conformational defects in odd-numbered alkanes“ [16,19]. The space group of phase O_{dci} was first determined by Nozaki et al. [20] for C25, and it corresponds to the space group of polyethylene.

It is believed that such a transition was first discovered by Snyder et al. [21] in the n-alkanes of C25, C27, C29 and was named the δ-transition. The authors observed a slight increase in the number of limit gauche defects at this transition using IR spectroscopy. This transition was first detected for C23 by Ungar [13] using the differential scanning calorimetry (DSC) and was categorized as a first-order transition. It was clarified by the author that the very small entropy of the transition cannot be associated with the acquisition of any new orientational degree of freedom. In addition, no changes in the position and intensity of the diffraction lines were observed.

However, Sirota et al. [2] were able to detect a slight increase in lamella thickness at this transition in the range from 31.09 to 31.20 Å. The authors concluded that these crystalline phases have the same packing of molecules in the lamellae (orthorhombic), but differ in the stacking of the lamellae relative to each other. The lamellae are stacked more densely in the low-temperature O_i phase compared to the high-temperature O_{dci} phase, which, as noted above, is consistent with the occurrence of gauche defects at the ends of the chains.

Similarly, Nozaki et al. [20] in defining the space group $Pbnm$ emphasized that its difference from the original group reflects a difference in the stacking of the molecular layers. Moreover, the structural changes at phase transitions $O_i \rightarrow O_{dci} \rightarrow R_V$ are mainly attributable to the change in the stacking of the molecular layers, which is affected by the degree of disordering on the lamella surface, i.e., the concentration of conformational defects at the ends of the chains. Interlamellar disordering, even if small, has a significant effect on the structure within the lamellae and leads to the formation of a new type of molecular stacking. In result, n-slip symmetry (along the diagonal of the lattice cell face) appears in the O_{dci} phase instead of c-slip symmetry (along the trans-zigzag axis) in the O_i phase.

In contrast, Blazquez-Blazquez et al. [18] did not detect any particular changes in the diffraction patterns, including an increase in lamellae thicknesses, but observed a slight

increase in the intensity of reflection 120 in case of the δ-transition. It was also found that reflection 120 completely disappears during the transition to the rotator phase R_V.

The appearance of a monoclinic phase was first found by Ungar [13] in C23 and C25. In addition, the space group Aa (9) was determined. Snyder et al. [21] also distinguished this phase in n-alkanes, starting at C25, by increase of the number of end gauche defects and named this transition γ. This phase was later labeled by M_{dci}.

It has been suggested [22] that molecules in the monoclinic phase M_{dci} make rotational jumps by 180° between two equally likely orientations, which excludes this crystal modification from the class of fully ordered phases. The designation R_V for the monoclinic phase as a rotator phase was first introduced by Sirota et al. [2] for n-alkanes C23–C27 when samples are cooled from the melt. It was found in the study that the phase transition $R_I \rightarrow R_V$ is a first-order transition for C23, in which there is a step-like change in the inclination of the molecules in the lamellae by about 4°. In addition, some coexistence of two phases such as R_I and R_V is noted. The thickness of the lamellae at this transition first decreases sharply by about 0.15 Å and then continues to decrease smoothly throughout the R_V phase with further cooling.

However, Sirota et al. [3] later attributed the $R_I \Rightarrow R_V$ transition to continuous transitions of the second order because of the absence of a sharp peak in heat capacity, based on the DSC data.

Ungar [13] found the phase R_V in C23 in the temperature interval of $\Delta T = 39.5–41\,^{\circ}\mathrm{C}$, which then transformed abruptly into the modification R_I. The author emphasized that the R_V structure is based on an orthorhombic type of subcell, but whose molecules appear to be crystallographically equivalent since there is no strict orientation of trans-zigzags of the „herringbone“ type. Crystallographic equivalence of molecules is a common feature of all plastic (rotator) modifications in n-alkanes.

Similar results for C23 upon heating were obtained by Nene et al. [17]. The authors confirmed the space group of the monoclinic R_V phase (Aa) and determined the lattice cell parameters. A continuous evolution of this phase was observed in the temperature range of $\Delta T = 40–42\,^{\circ}\mathrm{C}$. In this case, the authors assumed the martensitic-like nature of the (diffusionless) transition $R_V \rightarrow R_I$. It is argued that the remaining phase transitions in C23 are ordinary first-order transitions, which lead to significant changes in the crystal lattice and lattice cell volume.

We studied the thermodynamic properties of some n-alkanes in our previous papers [23,24] (with n from 16 to 25) using the DSC method. It was found that the transition from the solid state to the liquid state and back includes in two steps in even-numbered n-alkanes starting from C20 and in odd-numbered n-alkanes starting from C17, including C23, in heating-cooling cycles, i. e., a separate solid-solid phase transition comparable in enthalpy to melting/crystallization is distinguished. The presence of temperature hysteresis allowed referring this solid-solid phase transition to phase transitions of the first order. It was found that the solid-solid phase transition is diffuse and has a heterogeneous nature, i. e., it develops by fluctuating emergence of stable nanonuclei of a new phase in the volume of the preceding phase.

Dirand et al. [4] attributed this solid-solid phase transition to order-disorder transitions (o-d), because it involves significant changes in the orientation of molecules around their major axis (crystal axis c). The authors noted that the o-d transition is characterized by a higher thermal effect observed below the melting temperature than other solid-solid phase transitions. The authors assigned the less ordered phase, in which the molecules are oriented haphazardly around their major axis according to two equally likely positions in the subcell, to space group $Fmmm$. The monoclinic phase was distinguished by Dirand et al. in longer odd n-alkanes as ordered and did not record its occurrence in C23.

According to Nene et al. [17], further temperature increase to $T \sim 43\,^{\circ}\mathrm{C}$ leads to the appearance of a new polymorphic modification of C23 — phase R_I. This phase was identified by Ungar [13] as an orthorhombic rotator phase with space group $Fmmm$ (69). In the orthorhombic phase R_I, the lamellae stacking corresponds to the periodic sequence ABAB..., but the molecules are oriented haphazardly around their long axis according to four equally probable positions in the subcells. Thus, the molecules in lamellae A and B appear to be crystallographically equivalent, leading to the space group $Fmmm$ [4].

Ungar [13] found that the transverse dimensions of the lattice cell in the R_I phase undergo constant changes over a small temperature range, with the parameter ratio a/b sharply increasing with temperature, tending toward the value $\sqrt{3}$ that characterizes the hexagonal subcell. The parameter b decreases with temperature, as a consequence, the molecule in the neighboring lamella seems to be pushed out, resulting in a continuous increase of the interlamellar space in the R_I phase. Thus, as the temperature increases, the R_I phase gradually transforms towards hexagonal symmetry until reaching the ratio $a/b = 1.69$. Then an abrupt transition to a hexagonal modification R_{II} and a three-layer packing of lamellae takes place.

According to Nene et al. [17], a final modification of C23 is observed near $T \sim 46\,^{\circ}\mathrm{C}$ before melting. This structure was defined by Ungar [13] as a hexagonal (rhombohedral) rotator phase with space group $R\bar{3}m$ (166), subsequently designated R_{II}. The existence of this stable polymorphic modification with true hexagonal subcells was observed by Ungar for C23 and C25 in the temperature range of $\Delta T = 3–5\,^{\circ}\mathrm{C}$ before melting.

Ungar [13] observed that the $R_I \rightarrow R_{II}$ transition does not significantly increase the interlamellar space or cross-sectional area of the chain, consistent with the very small latent heat of transition observed in the DSC thermograms.

Thus, the following sequence of phase states of tricosane upon heating can be expected based on the body of literature data: low-temperature orthorhombic crystalline

Table 1. The lattice cell parameters of the polymorphic modifications of tricosane C23

Phase, its Bravais lattice, and space group	Parameters lattice cell	
O_i, PO, P_{bcm} (57)	$a = 4.970 \pm 0.005$ Å, $b = 7.478 \pm 0.005$ Å, $c = 62.31 \pm 0.10$ Å, angle of inclination of plane trans-zigzag to axis a: $\theta = (48 \pm 5)^\circ$	[15]
	$a = 4.967 \pm 0.002$ Å, $b = 7.441 \pm 0.004$ Å, $c = 62.189 \pm 0.020$ Å	[25]
	$a = 7.467 \pm 0.008$ Å, $b = 4.983 \pm 0.007$ Å, $c = 62.19 \pm 0.04$ Å	[16]
	$a = 7.472 \pm 0.008$ Å, $b = 4.945 \pm 0.008$ Å, $c = 62.02 \pm 0.04$ Å	[17]
O_{dci}, PO, P_{bnm} (62)	$a = 7.546 \pm 0.008$ Å, $b = 4.989 \pm 0.007$ Å, $c = 62.26 \pm 0.04$ Å	[16]
	$a = 7.419 \pm 0.015$ Å, $b = 4.980 \pm 0.010$ Å, $c = 62.05 \pm 0.11$ Å	[17]
R_V, M_{dci}, CM, Aa (9)	$a = 7.93 \pm 0.37$ Å, $b = 4.94 \pm 0.11$ Å, $c = 62.6 \pm 1.5$ Å, $\beta = (86 \pm 14)^\circ$	[17]
R_I, FCO, $Fmmm$ (69)	$a = 8.074 \pm 0.008$ Å, $b = 4.843 \pm 0.007$ Å, $c = 62.63 \pm 0.05$ Å	[17]
R_{II}, Rh, $R\bar{3}m$ (166)	$a = 4.76$ Å, $c = 95.1$ Å, $\gamma = 120^\circ$	[13]
	$a = 4.769 \pm 0.007$ Å, $c = 94.14 \pm 0.16$ Å, $\gamma = 120^\circ$	[17]

Note. Bravais lattice designations: PO — primitive orthorhombic; CM — base-centered monoclinic; FCO — face-centered orthorhombic; Rh — rhombohedral (twice volume-centered hexagonal).

phase $O_i \rightarrow$ high-temperature orthorhombic crystalline phase $O_{dci} \rightarrow$ monoclinic rotator phase $R_V \rightarrow$ orthorhombic rotator phase $R_I \rightarrow$ rhombohedral (hexagonal) rotator phase $R_{II} \rightarrow$ liquid.

Literature data on the lattice cell parameters of all polymorphic modifications of tricosane C23 are provided in Table 1.

It can be concluded that at present the sequence of phase states of C23 upon heating has been determined quite reliably, but there are many contradictions about the course of phase transformations in the solid state.

The aim of this study is to establish the kinetics of polymorphic transformations of C23 tricosane upon heating, i.e., to study the process of transition of some phases into others, which will help to eliminate the gaps in understanding the mechanism of structural rearrangements in n-alkanes.

3. Experimental part

Samples of monodispersed (purity 99%) tricosane n-$C_{23}H_{48}$ produced by Sigma-Aldrich were studied.

Thermal analysis was performed using Henven HSC-4 differential scanning calorimeter (China) in a nitrogen atmosphere. The weight of the test sample was 10.2 mg, which is sufficient to detect weak thermal effects during phase transitions while ensuring that the thermal resistance of the calorimetric cell is minimized to reduce methodological error. The sample for the study was prepared as follows: fine flakes of Sigma-Aldrich tricosane synthesis products were selected and then placed in a calorimetric cuvette and covered with a lid without additional pressing to prevent structural changes. The scanning speed was chosen 0.5 °C/min, optimal for samples of a given mass, to ensure that the intensity of the weak heat capacity peaks and their resolution on the temperature scale during heating were sufficient to be recorded.

For X-ray diffraction studies, the sample was placed in a quartz capillary from Capillary Tube Supplies Ltd, UK with an outside diameter of 0.3 mm and wall thickness of 10 μm. A small sample suspension was placed into the expanded portion of the capillary using tweezers and then heated with a stream of warm air until molten (about 50 °C). The tricosane melt filled a narrow part of the capillary and then crystallized upon natural cooling to room temperature.

X-ray diffraction studies were performed in X-ray diffraction analysis (BELOK-RSA) station of Kurchatov Synchrotron Radiation Source „KISI-Kurchatov“ [26] equipped with a Rayonix SX165 two-dimensional CCD detector ($\lambda = 0.75$ Å, Si monochromator). Measurements were performed in transmission geometry, the detector was placed at a distance of 80.5 mm from the sample, and the X-ray beam cross-section was 0.4×0.4 mm. Diffraction patterns were taken twice to improve the statistics during the diffraction pattern accumulation time of $t = 9$ s.

In the study of the structural transformations of tricosane, diffraction patterns were recorded under conditions of linear heating of the capillary with the sample in the temperature range of $\Delta T = 35-48$ °C at a rate 0.4 °C/min, close to the heating rate in the DSC method (0.5 °C/min). The temperature interval for the X-ray diffraction studies was chosen according to the thermal effects observed in the DSC thermograms (see results and discussion). Temperature was controlled using a Cryostream 700Plus device (Oxford cryosystems) with an accuracy of ± 0.1 °C. The sample temperature changed by $\Delta T = 0.1$ °C at a given heating rate during the signal accumulation time of 9 s and 6 s during

the 2D diffraction pattern storage time, which corresponds to the period of diffraction pattern recording. A large array of 2D diffraction patterns was thus obtained, each corresponding to a temperature change in the interval $\Delta T = 0.06\,^{\circ}\mathrm{C}$.

The 2D diffraction patterns obtained over the entire temperature range were reduced to the one-dimensional form of the dependence of the diffracted beam intensity on the double diffraction angle $I(2\theta)$ using azimuthal integration in Dionis — Diffraction Open Integration Software [27]. The obtained one-dimensional dependences $I(2\theta)$ were then normalized to the current intensity of the primary synchrotron X-ray beam. Hardware broadening of diffraction lines was accounted for by measuring the certified standard LaB_6 (NIST SRM 660a).

4. Results and discussion

The heating thermogram of C23 tricosane in the temperature range of $\Delta T = 35-53\,^{\circ}\mathrm{C}$ corresponding to the phase transition is shown in Figure 1. Two base peaks of heat capacity corresponding to solid-solid phase transition and melting can be seen on this dependence. The considered solid-solid phase transition is a diffuse first-order phase transition, which was established in our previous papers [23,24].

Sufficient mass of the sample and high sensitivity of the instrument allowed us to detect a number of weak thermal effects in the interval $\Delta T = 37-46\,^{\circ}\mathrm{C}$, manifested in the deviation of the heat capacity curve from the baseline. To establish the nature of the observed effects, synchrotron X-ray diffractometry studies were carried out when the sample was heated at a rate close to the heating rate when the DSC thermogram was recorded (see experimental part).

Figure 2 shows selected 2D diffraction patterns of tricosane obtained by heating the sample up to the melting point. It can be seen that there are significant changes in the structure over the entire temperature range: the number of arcs close to the center of the diffraction pattern gradually decreases (small-angle reflections), the rings of the highest intensity are displaced (large-angle reflections), and the semicircles distant from the center of the pattern disappear (higher-order reflections). Detailed discussions of the observed effects are presented below.

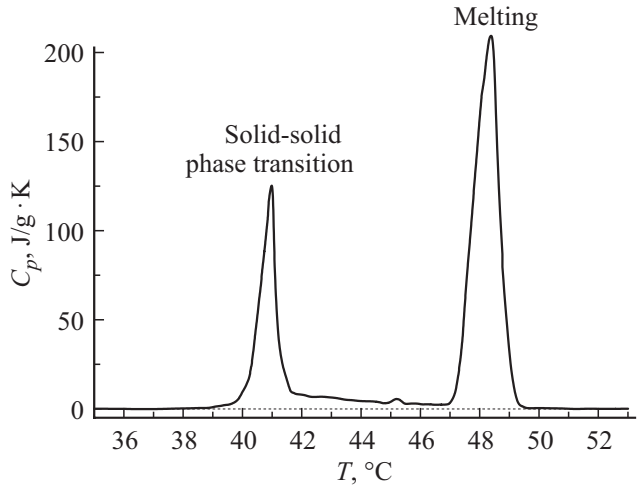

Figure 1. Thermogram of tricosane heating at a rate of 0.5 K/min.

Table 2. Positions of the observed reflections in the low-temperature orthorhombic phase O_i of tricosane at $T = 35.3\,^{\circ}\mathrm{C}$

Miller indices *hkl*	Reflection position 2θ, deg ($\lambda = 0.75$ Å)
002	1.33
004	2.70
006	4.07
008	5.47
110	10.40
115	10.95
020	11.50
120	14.39

The diffraction patterns at small angles (Figure 2) clearly show a series of arcs (reflections) corresponding to reflections 00*l*. It should be noted that about seven orders of diffraction in small angles are observed at low temperatures (Figure 2, *a, b*), and their number decreases to at least four when heated (Figure 2, *c, d, e*). Since n-alkanes tend to form lamellar crystals whose axis *c* is perpendicular to the basic lamellae planes, the parameter *c* of the main lattice cell determines the position of the reflections 00*l*. The large number of orders of small-angle reflections indicates the presence of extended regular stacks of numerous layered nanolamellae.

The stacking of lamellae relative to each other is bilayer in the initial orthorhombic structure O_i of tricosane [15]. Thus, the parameter *c*, defined by the distance between neighboring reflections 00*l* at $l = 2n$, corresponds to twice the length of a fully extended C23 molecule.

The large-angle reflections (rings) (Figure 2) are attributable to subcell symmetry in the crystal cores of the lamellae. The initial C23 orthorhombic subcells are characterized by the presence of two strong reflections in the diffraction patterns — 110 and 020, allowing us to determine the parameters *a* and *b* of the lattice cells to a first approximation.

The angular positions of the main observed reflections in the low-temperature orthorhombic phase O_i for C23 are presented in Table 2.

A decrease in the intensity of the reflections 110 and 020 and their shift towards smaller angles in the temperature range of $\Delta T = 35.3-38.2\,^{\circ}\mathrm{C}$ are observed in the initial phase O_i in case of heating of C23, (Figure 3). The intensity of both reflections jumps at temperature of $T = 38.3\,^{\circ}\mathrm{C}$, which may indicate the transition of C23 into the high-temperature orthorhombic phase O_{dci}.

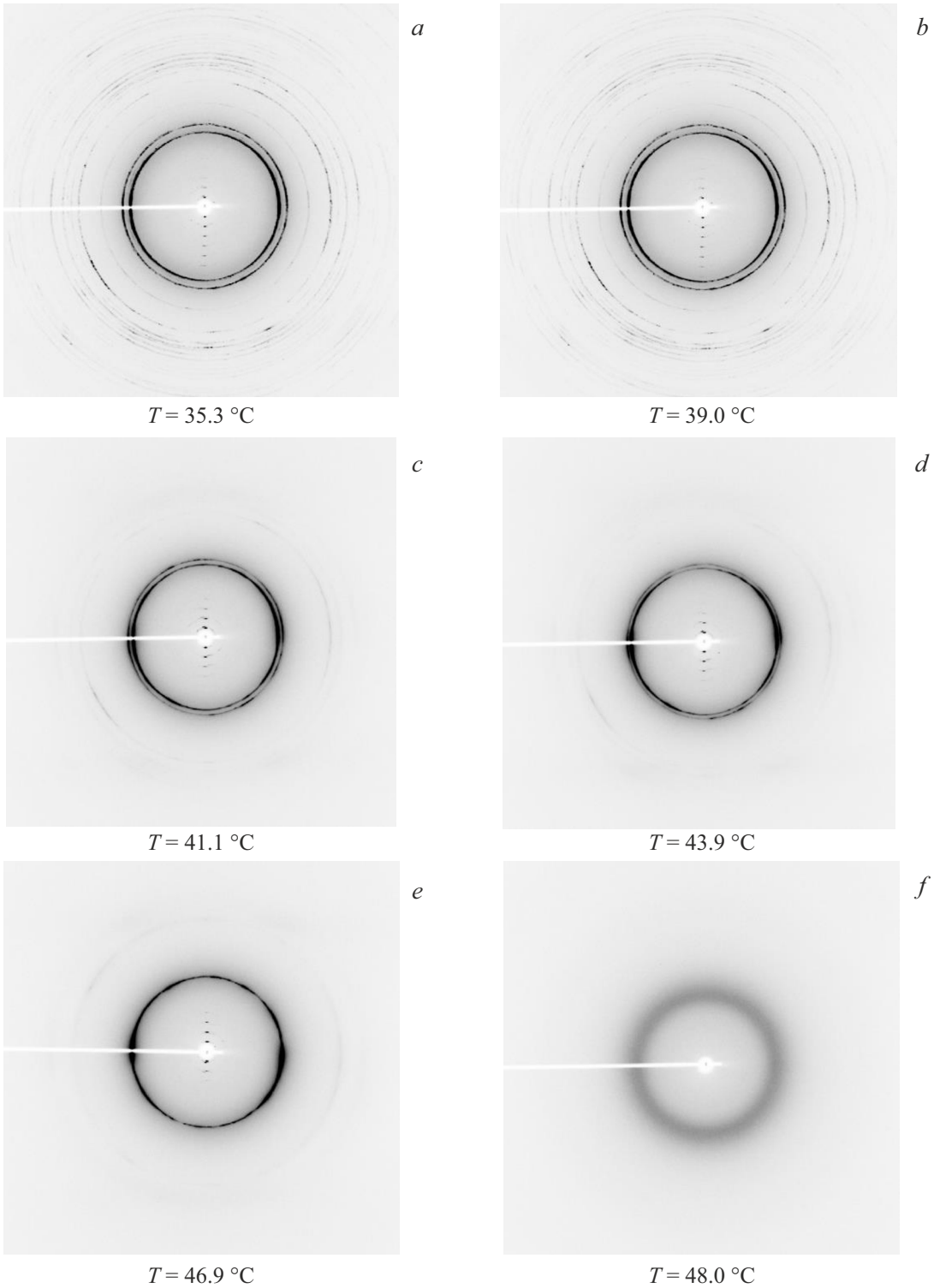

Figure 2. 2D-diffraction patterns of tricosane, each obtained in the heating interval $\Delta T = 0.06\,^{\circ}\mathrm{C}$ and labeled by mean temperature: 35.3 (*a*), 39.0 (*b*), 41.1 (*c*), 43.9 (*d*), 46.9 (*e*), 48.0 °C (*f*).

As mentioned above, Blazquez-Blazquez et al. [18] found a slight increase in the intensity of reflection 120 in case of the transition $O_i \rightarrow O_{dci}$, and found it to disappear completely in case of the rotator phase transition R_V, but did not record changes in reflections 110 and 020, which are observed in Figure 3. In addition, our data also confirm the change in the intensity of reflection 120 at temperature of $T = 38.3\,^{\circ}\mathrm{C}$ (Figure 4).

Thus, a transition of one orthorhombic phase to another with a change in space group ($P_{bcm} \rightarrow P_{bnm}$) takes place

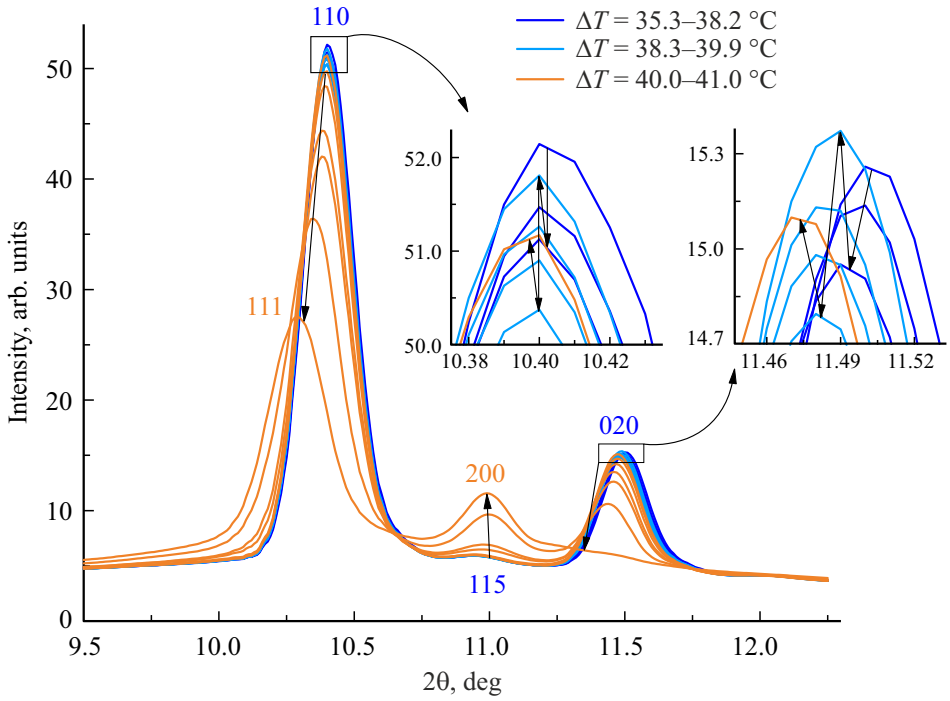

Figure 3. Temperature changes of tricosane diffraction patterns in case of heating in the temperature range of $\Delta T = 35.3-41.0\,^{\circ}C$. The insets show the reflection changes in more detail. Arrows indicate directions of change with heating. Diffraction patterns of phase O_i are shown by dark blue color, diffraction patterns of phase O_{dci} are shown by light blue color, coexistence of phases O_{dci} and R_V is shown by orange color.

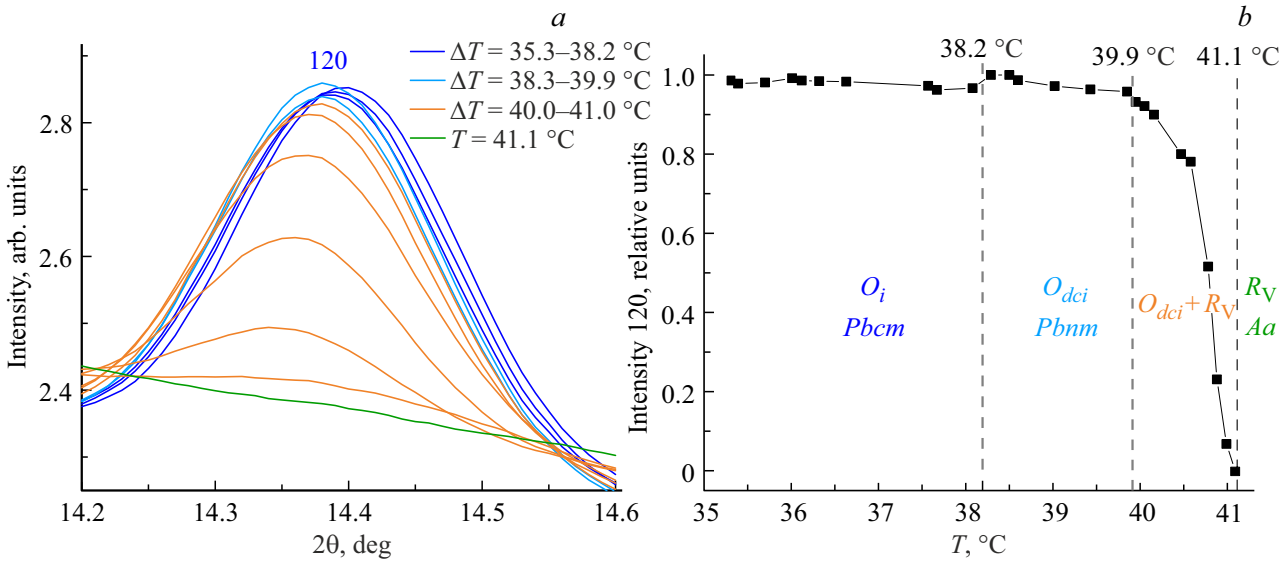

Figure 4. *a* — temperature changes of the diffraction patterns in the region of the reflection 120 and *b* — change in the intensity of the corresponding reflection for tricosane when heated in the temperature range $\Delta T = 35.3-41.1\,^{\circ}C$.

at temperature of $T = 38.1-38.3\,^{\circ}C$. Table 3 presents the angular positions of the observed reflections of the high-temperature orthorhombic phase O_{dci} in C23.

We again observe a decrease in the intensity in the phase O_{dci} in case of heating of C23 in the temperature range of $\Delta T = 38.3-39.9\,^{\circ}C$, but already the reflections 111 and 200, characteristic of the lattice cells of the new space group, and their shift towards smaller angles (Figure 3).

The intensity of both reflections again jumps at temperature of $T = 40.0\,^{\circ}C$ (Figure 3), which we believe indicates the following phase transition. Moreover, the orthorhombic phase reflections 111 and 200 undergo significant changes in

Table 3. Positions of observed reflections in the high-temperature orthorhombic phase O_{dci} of tricosane at $T = 39.0\,^{\circ}\mathrm{C}$

Miller indices *hkl*	Reflection position 2θ, deg ($\lambda = 0.75\,\text{Å}$)
002	1.33
004	2.70
006	4.07
008	5.46
111	10.40
115	10.94
200	11.49
210	14.38

Table 4. Positions of the observed reflections in the monoclinic rotator phase R_V of tricosane at $T = 41.1\,^{\circ}\mathrm{C}$

Miller indices *hkl*	Reflection position 2θ, deg ($\lambda = 0.75\,\text{Å}$)
002	1.33
004	2.70
006	4.07
008	5.47
111	10.27
200	10.97

the temperature interval of $\Delta T = 40.0{-}41.0\,^{\circ}\mathrm{C}$ associated with a gradual decrease in their intensity, but a completely new reflection 200 corresponding to the appearance of lattice cells of monoclinic symmetry appears and intensifies. Thus, the coexistence of orthorhombic and monoclinic phases was found in the narrow temperature range of $\Delta T \sim 1\,^{\circ}\mathrm{C}$, which is a direct confirmation of the results obtained by the DSC method about the heterogeneous course of the solid-solid phase transition by formation of nuclei of a new phase in the volume of the preceding one.

In addition, the gradual disappearance of the domains of the true orthorhombic phase with molecule packing in „herringbone“ subcells is confirmed by the gradual weakening of the reflection 120 and its complete disappearance at temperature of $T = 41.1\,^{\circ}\mathrm{C}$. This effect can be explained by the appearance of some freedom of rotation of molecules around their long axes in the subcells of crystal nucleations of the monoclinic phase, which allows us to characterize it as rotator phase. At the same time, in-phase with gradual changes in the reflections 111, 200 and 120 disappear and higher-order reflections in large angles (Figure 2), which also indicates the transition to the rotator phase, which is accompanied by an increase in the degree of crystalline disorder [13]. In addition, the number of orders of small-angle reflections sharply decreases at $T = 41.0\,^{\circ}\mathrm{C}$, indicating an increase in the degree of lamella stacking disorder. Ungar [13] also observed that the integral intensity and number of small-angle reflections $00l$ significantly decreases during the transition from crystalline orthorhombic phases to rotator phases. This fact can be attributed to the appearance of „roughness“ on the lamellar surface in the rotator phases and, as a consequence, to some increase in the interlamellar space, which is consistent with the appearance of conformational defects at the ends of the chains.

It can be concluded that the pure monoclinic rotator phase R_V appears at $T = 41.1\,^{\circ}\mathrm{C}$. The angular positions of the observed reflections in the monoclinic rotator phase R_V for C23 are presented in Table 4.

The monoclinic rotator phase R_V exists in the extremely narrow temperature range of $\Delta T = 41.1{-}41.2\,^{\circ}\mathrm{C}$, since a shift of the reflection 200 towards smaller angles is observed already at $T = 41.3\,^{\circ}\mathrm{C}$ while the position of the reflection 111 does not change (Figure 5). This change in the diffraction patterns continues in the temperature range of $\Delta T = 41.3{-}41.8\,^{\circ}\mathrm{C}$.

The reflection 200 continues to shift toward smaller angles with further temperature increase in the temperature interval of $\Delta T = 41.9{-}44.9\,^{\circ}\mathrm{C}$, while reflection 111 begins to move toward higher angles (Figure 5). The reflections merge into one at $T = 45.0\,^{\circ}\mathrm{C}$. This behavior of the diffraction pattern is characteristic of the orthorhombic rotator phase R_I [13]. It can be assumed that the changes occurring in the interval of $\Delta T = 41.3{-}41.8\,^{\circ}\mathrm{C}$ are attributable to the continuity of the second-order phase transition $R_V \Rightarrow R_I$ and can be explained by the intermediate state between R_V and R_I and the impossibility of separating one phase from the other.

The angular positions of the observed reflections in the orthorhombic rotator phase R_I for C23 are listed in Table 5.

As noted above, the two strong reflections 111 and 200 merge into a single reflection 101 at $T = 45.0\,^{\circ}\mathrm{C}$ (Figure 5). A rather abrupt transition to the final hexagonal modification of the tricosane — to the rotator phase R_{II} takes place at this point. However, an arm is still observed at the reflection 101 on the large angle side in the temperature range of $\Delta T = 45.1{-}45.3\,^{\circ}\mathrm{C}$ (Figure 6), indicating a residual contribution of the reflection 200 of the orthorhombic phase R_I. Thus, the coexistence of two phases R_I and R_{II} is revealed in the temperature range of $\Delta T = 45.0{-}45.3\,^{\circ}\mathrm{C}$. The heterogeneous nature of the development of the phase transition $R_I \rightarrow R_{II}$ in the narrow temperature range of $\Delta T \approx 0.3\,^{\circ}\mathrm{C}$ can be inferred based on this.

The existence of stable rhombohedral (hexagonal) rotator phase R_{II} is observed during the subsequent temperature increase in the interval of $\Delta T = 45.4{-}47.0\,^{\circ}\mathrm{C}$ (Figure 6). The angular positions of the observed reflections of high-temperature rotator phase R_{II} for C23 are listed in Table 6.

Finally, reflection 101 smoothly weakens and shifts toward smaller angles upon further heating of C23 in the temperature range of $\Delta T = 47.1{-}48.0\,^{\circ}\mathrm{C}$ (Figure 6), indicating a gradual transition to a disordered state, i. e., melting of the sample. Only an amorphous halo is observed at $T = 48.0\,^{\circ}\mathrm{C}$.

The interplanar distances d_{hkl} corresponding to the observed reflections can be determined for the diffraction maxima $2d \sin\theta = n\lambda$ from the Bragg-Wulff condition. The relationship between the observed reflections and the lattice

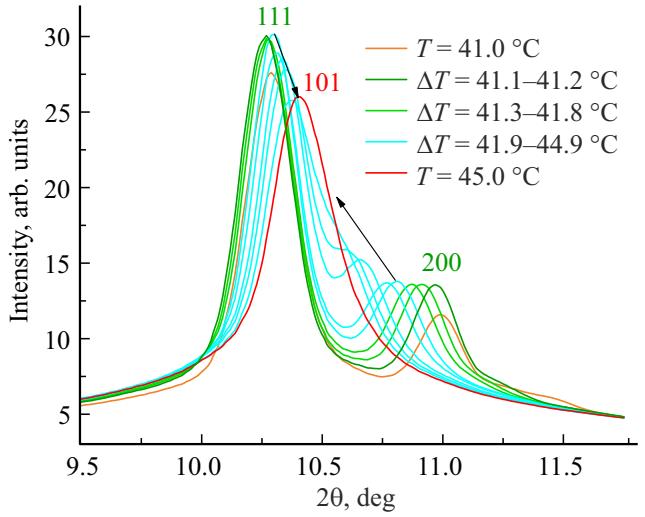

Figure 5. Temperature changes of tricosane diffraction patterns upon heating in the temperature range of $\Delta T = 41.0-45.0\,^{\circ}$C. Arrows indicate directions of change with heating. Diffraction patterns of coexistence of phases O_{dci} and R_V are shown by the orange color, diffraction patterns of phase R_V are shown by green color, intermediate state between R_V and R_I are shown by light green color, diffraction patterns of phase R_I are shown by turquoise color, diffraction patterns of coexistence of phases R_I and R_{II} are shown by red color.

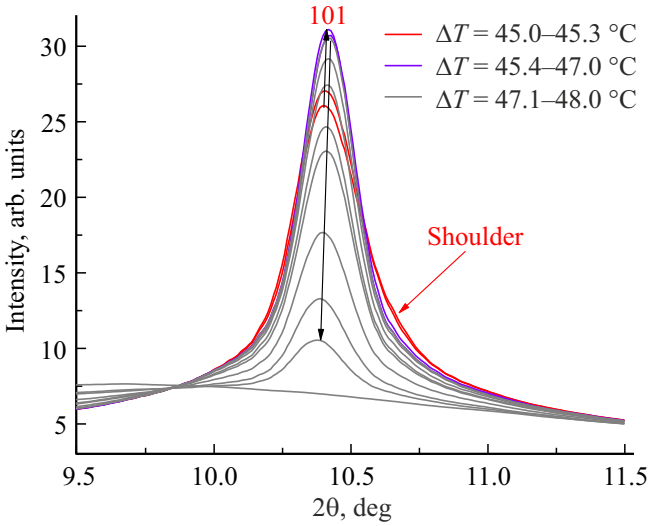

Figure 6. Temperature changes of tricosane diffraction patterns upon heating in the temperature range of $\Delta T = 45.0-48.0\,^{\circ}$C. Black arrows indicate directions of change upon heating. The red arrow emphasizes the presence of a shoulder at reflection 101 due to residuals of the orthorhombic phase. Diffraction patterns of the coexistence of phases R_I and R_{II} are shown by red color, diffraction patterns of phase R_{II} are shown by purple color, diffraction patterns of melting of the sample are shown by gray color.

Table 5. Positions of observed reflections in the orthorhombic rotator phase R_I of tricosane at $T = 43.9\,^{\circ}$C

Miller indices *hkl*	Reflection position 2θ, deg ($\lambda = 0.75$ Å)
002	1.33
004	2.67
006	4.03
111	10.34
200	10.65

Table 6. Positions of observed reflections in the rhombohedral (hexagonal) rotator phase R_{II} of tricosane at $T = 46.0\,^{\circ}$C

Miller indices *hkl*	Reflection position 2θ, deg ($\lambda = 0.75$ Å)
002	1.35
004	2.67
006	4.03
101	10.42

cell parameters can be represented in general terms by an expression for the interplanar distance d_{hkl} in the triclinic structure [28], which is simplified for higher syngonies.
For the orthorhombic structure ($\alpha = \beta = \gamma = 90^{\circ}$) we obtain:

$$\frac{1}{d_{hkl}^2} = \frac{h^2}{a^2} + \frac{k^2}{b^2} + \frac{l^2}{c^2}. \quad (1)$$

For the monoclinic structure ($\alpha = \gamma = 90^{\circ}$):

$$\frac{1}{d_{hkl}^2} = \frac{h^2}{a^2(\sin\beta)^2} + \frac{k^2}{b^2} + \frac{l^2}{c^2(\sin\beta)^2} - \frac{2hl\cos\beta}{ac(\sin\beta)^2}. \quad (2)$$

For hexagonal structure ($a = b$, $\alpha = \beta = 90^{\circ}$, $\gamma = 120^{\circ}$):

$$\frac{1}{d_{hkl}^2} = \frac{4}{3}\frac{h^2 + k^2 + hk}{a^2} + \frac{l^2}{c^2}. \quad (3)$$

Thus, the lattice cell parameters of each of the polymorphic modifications of tricosane upon heating were calculated based on the angular positions of the observed reflections and the expressions (1)–(3). Figure 7 shows the temperature changes of the parameters a and b for all phase states of C23. The lattice cell parameters we have determined are in agreement with the values presented earlier in Table 1.

Figure 7 shows that the parameters a and b remain nearly constant in the orthorhombic phases O_i and O_{dci}. The appearance of nuclei of monoclinic rotator phase R_V at $T = 39.9\,^{\circ}$C initiates a slight increase in the lattice cell parameters of the phase O_{dci}. The increase in the number of monoclinic phase nuclei as the phase transition progresses leads to a significant stretching of the lattice cells of both phases along the parameter b, i. e., the new phase nuclei significantly deform the molecular crystals. It should be

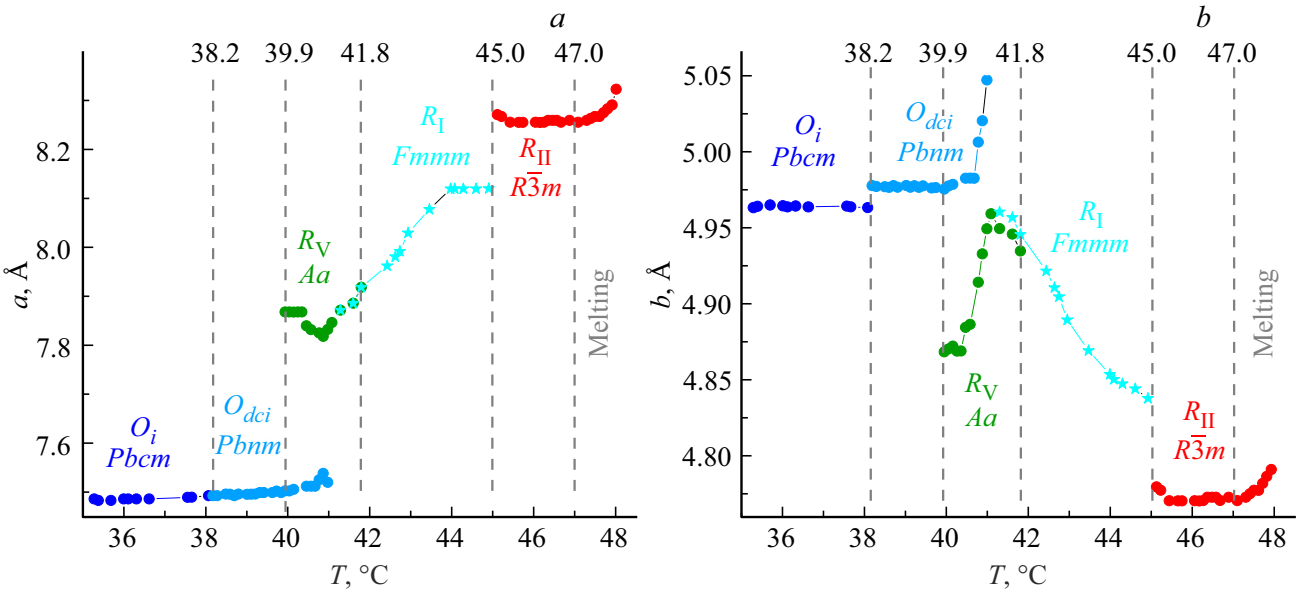

Figure 7. Temperature changes of the parameters a (a) and b (b) of the lattice cells of polymorphic modifications of tricosane in case of heating in the temperature range of $\Delta T = 35.0-48.0\,^{\circ}\mathrm{C}$.

noted that the calculated inclination angle of the molecules relative to the lamellae reference planes in the monoclinic phase is only 2.2°. The lattice cell parameters of the phase R_V begin to undergo small changes At $T = 41.1\,^{\circ}\mathrm{C}$ that continue into the interval of $\Delta T = 41.3-41.8\,^{\circ}\mathrm{C}$, which corresponds to the intermediate state between R_V and R_I in case of the second-order phase transition. The lattice cells become orthorhombic again in the result of the transition, which accounts for the occurrence of the rotator phase R_I. A permanent transformation of the lattice cells of the phase R_I takes place upon further heating in the interval of $\Delta T = 41.9-44.9\,^{\circ}\mathrm{C}$. Then, a new phase transition occurs in the temperature range of $\Delta T = 45.0-45.3\,^{\circ}\mathrm{C}$ with the emergence of hexagonal phase nuclei R_{II}. Hexagonal packing of molecules with nearly constant lattice cell parameters is preserved in the temperature interval of $\Delta T = 45.4-47.0\,^{\circ}\mathrm{C}$. Then, the gradual expansion of the lattice cells begins in the temperature range of $\Delta T = 47.1-48.0\,^{\circ}\mathrm{C}$, eventually leading to a transition to a disordered, liquid state (melt).

Figure 8, a shows the temperature changes of the lattice cell parameter ratio a/b in all polymorphic modifications of tricosane C23. It can be seen that the non-rotator crystalline phases O_i and O_{dci} are characterized by the parameter ratio $a/b \approx 1.51$. During the transition to the rotator phase, a/b increases by a jump and continues to increase to a value of 1.68 throughout the phase R_I. Then the ratio a/b changes again by jump tending to the value $\sqrt{3}$, which characterizes the hexagonal symmetry of the subcells.

Based on the results obtained by synchrotron X-ray diffractometry, we were able to establish the nature of the weak thermal effects observed in Figure 1 for C23 upon heating. Figure 8, b shows the thermogram of tricosane heating with correlation between the observed thermal effects and the sequence of polymorphic modifications established above.

It can be seen from Figure 8, b that the phase transition from the initial phase O_i to O_{dci} appears as a small jump in heat capacity relative to the baseline. A broad and intense heat capacity peak is then observed, characterizing a diffuse first-order solid-solid phase transition, which corresponds to the gradual transformation of the phase O_{dci} into R_V. The above-established coexistence of two phases at this solid-solid phase transition confirms the heterogeneous nature of its development, i.e., the formation of nuclei of a new phase in the volume of the preceding phase, which was established by us earlier [24] on the basis of analyzing the shape of the heat capacity peak according to the theory of diffuse phase transitions [29,30]. The narrow temperature interval of existence of phase R_V is not reflected in the DSC thermogram, which may be attributable to its continuous transition to phase R_I. The permanent transformation of the phase R_I revealed from the X-ray data upon heating appears on the thermogram as a gradual decline in heat capacity. The next transition from phase R_I to phase R_{II} presents a small symmetric heat capacity peak, which can be attributed to diffuse phase transitions, which confirms the assumption made above about the heterogeneous nature of the course of the phase transition $R_I \rightarrow R_{II}$. A large peak in heat capacity is further observed along the temperature (see also Figure 1), corresponding to the melting of the sample.

As can be seen from the comparison of Figure 8, a, b, there is a good correspondence between the temperature intervals for the existence of polymorphic modifications established by synchrotron X-ray diffractometry and differential scanning calorimetry.

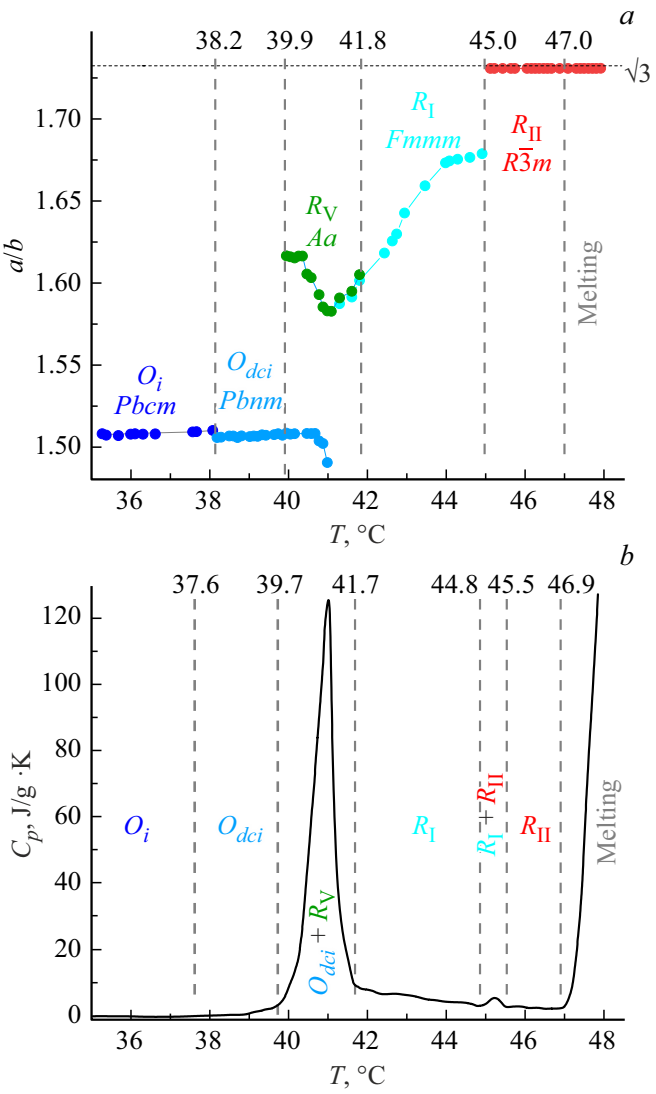

Figure 8. *a* — temperature changes of the lattice cell parameter ratio a/b of polymorphic modifications of tricosane upon heating in the temperature range of $\Delta T = 35.0-48.0\,^{\circ}$C; *b* — polymorphic modifications of tricosane on DSC thermogram.

The highest intensity of the heat capacity peak of the transition $O_{dci} \rightarrow R_V$ compared to the other solid-solid phase transitions attracts attention (Figure 8, *b*). A characteristic feature of this transition is the activation of collective rotational motions of n-alkane molecules around the principal axes of trans-zigzags with rotations by discrete angles. It is the appearance of molecular rotation throughout the crystal volume that helps to explain the high value of the solid-solid phase transition heat capacity peak. Similarly, when the aggregation state of the n-alkane changes (melting), the molecules acquire complete freedom of motion, which corresponds to an even higher intensity of the heat capacity peak. It should be noted that the change of structural parameters (sizes of elementary cells) at other solid-solid phase transitions does not require such a large energy absorption, which is manifested on DSC thermograms in the form of weak endothermic effects. It can be assumed that increasing the sensitivity of the DSC instrument will allow clearly distinguishing these effects against the background of highly intense heat capacity peaks and to study in more detail solid-solid phase transitions with low energy absorption.

5. Conclusion

Polymorphic transformations in monodisperse samples of tricosane n-$C_{23}H_{48}$ heated from room temperature to melt temperature ($T_m = 48.0\,^{\circ}$C) have been studied by synchrotron X-ray diffractometry and differential scanning calorimetry methods.

X-ray diffraction studies of tricosane were first performed during continuous linear heating of the sample at a rate of $0.4\,^{\circ}$C/min. The short signal accumulation time ($t = 9$ s) made it possible to obtain a large array of 2D diffraction patterns, each corresponding to a temperature change of $\Delta T = 0.06\,^{\circ}$C.

It is shown that the transition from the solid state to the melt is accomplished in the n-alkane n-$C_{23}H_{48}$ by at least five consecutive phase transitions of different nature, capturing a wide temperature interval of $\Delta T = 35-50\,^{\circ}$C.

The first of the sequence of phase transitions upon heating of tricosane is observed to be a first-order solid-solid phase transition in a narrow temperature range of $\Delta T = 38.1-38.3\,^{\circ}$C, due to the change of symmetry P_{bcm} of the original orthorhombic cells (O_i) to a higher temperature P_{bnm} (O_{dci}).

The heterogeneous nature of the following solid-solid phase transition was first detected by synchrotron X-ray diffractometry. Nanonuclei of the monoclinic rotator phase R_V, characterized by thermal activation of retarded discrete rotation of molecules around their principal axes, arise and propagate in the volume of the high-temperature orthorhombic phase O_{dci} in the temperature interval of $\Delta T = 40.0-41.1\,^{\circ}$C. The pure rotator phase R_V is found to be stable only in a very narrow temperature range of $\Delta T = 41.1-41.2\,^{\circ}$C. It is found that with the appearance of the rotational ability of the molecules, there is an increase in the degree of disorder in the crystal cores of the nanolamellae, and the regularity of the mutual stacking of the lamellae in the stacks is disturbed.

In the temperature region of $\Delta T = 41.3-41.8\,^{\circ}$C in n-alkane n-$C_{23}H_{48}$ small changes in the lattice cell parameters of the phase R_V occur, leading to values characteristic of the orthorhombic rotator phase R_I. In our opinion, the observed structural transformations correspond to the development of a continuous second-order phase transition between two rotator phases, $R_V \Rightarrow R_I$, since one or the other phase cannot be unambiguously distinguished at the phase transition point.

The rotator phase R_I is found in the temperature range of $\Delta T = 41.9-44.9\,^{\circ}$C. This phase is characterized by continuous changes in the lattice cell parameters over the

entire temperature interval, on the basis of which the phase R_I can be considered metastable. Then, the parameter ratio a/b reaches the value of $\sqrt{3}$ at $T = 45.0\,^{\circ}\mathrm{C}$, which is characteristic of the hexagonal packing type of n-alkane molecules. We attribute this effect to the fact that nuclei of the hexagonal rotator phase R_{II} arise in the volume of phase R_I in the interval of $\Delta T = 45.0{-}45.3\,^{\circ}\mathrm{C}$. Thus, the heterogeneous nature of the first-order solid-solid phase transition $R_I \rightarrow R_{II}$ is established for the first time.

A stable rhombohedral (hexagonal) rotator phase R_{II} with unchanged lattice cell parameters is observed in the temperature range of $\Delta T = 45.4{-}47.0\,^{\circ}\mathrm{C}$. Only then, in the temperature range of $\Delta T = 47.1{-}48.0\,^{\circ}\mathrm{C}$ does the gradual expansion of the hexagonal cells begin, eventually leading to the transition to the disordered, liquid state (melt).

Thus, the kinetics of the development of a sequence of phase transitions of different nature in tricosane n-$C_{23}H_{48}$ has been revealed for the first time: low-temperature orthorhombic crystalline phase $O_i \rightarrow$ high-temperature orthorhombic crystalline phase $O_{dci} \rightarrow$ monoclinic rotator phase $R_V \Rightarrow$ orthorhombic rotator phase $R_I \rightarrow$ rhombohedral (hexagonal) rotator phase $R_{II} \rightarrow$ liquid. A strict attribution of the observed phase transitions to either diffuse first-order phase transition ($O_{dci} \rightarrow R_V$, $R_I \rightarrow R_{II}$) in which the two phases coexist has been carried out; or to phase transitions of the second order ($R_V \Rightarrow R_I$), at which the symmetry of the lattice cell changes continuously.

In all phase states, the lattice cell parameters and, moreover, for the first time their temperature changes in each of the polymorphic modifications of tricosane n-$C_{23}H_{48}$ have been determined.

Conflict of interest

The authors declare no conflict of interest.

References

[1] M.G. Broadhurst. J. Res. Natl. Bur. Stand. **66A**, *3*, 241 (1962).
[2] E.B. Sirota, H.E. King, D.M. Singer, H.H. Shao. J. Chem. Phys. **98**, *7*, 5809 (1993).
[3] E.B. Sirota, D.M. Singer. J. Chem. Phys. **101**, *12*, 10873 (1994).
[4] M. Dirand, M. Bouroukba, V. Chevallier, D. Petitjean, E. Behar, V. Ruffier-Meray. J. Chem. Eng. Data **47**, *2*, 115 (2002).
[5] A.-J. Briard, M. Bouroukba, D. Petitjean, N. Hubert, M. Dirand. J. Chem. Eng. Data **48**, *3*, 497 (2003).
[6] D. Cholakova, K. Tsvetkova, S. Tcholakova, N. Denkov. Colloids Surf. A: Physicochem. Eng. Asp. **634**, 127926 (2022).
[7] A.K. Borisov, S.A. Gureva, V.M. Egorov, V.A. Marikhin. FTT **66**, *10*, 1810 (2024).
[8] A. Müller. Proc. Royal Soc. **A138**, *836*, 514 (1932).
[9] A.I. Kitaigorodsky. Molekulyarnyye kristally. Nauka, M. (1971). (in Russian). 424 p.
[10] J. Doucet, I. Denicoló, A.F. Craievich. J. Chem. Phys. **75**, *3*, 1523 (1981).
[11] J. Doucet, I. Denicoló, A.F. Craievich, A. Collet. J. Chem. Phys. **75**, *10*, 5125 (1981).
[12] I. Denicoló, J. Doucet, A.F. Craievich. J. Chem. Phys. **78**, *3*, 1465 (1983).
[13] G. Ungar. J. Phys. Chem. **87**, *4*, 689 (1983).
[14] J. Doucet, I. Denicoló, A.F. Craievich, C. Germain. J. Chem. Phys. **80**, *4*, 1647 (1984).
[15] A.E. Smith. J. Chem. Phys. **21**, 2229 (1953).
[16] L. Robles, D. Mondieig, Y. Haget, M.A. Cuevas-Diarte. J. Chim. Phys. **95**, 92 (1998).
[17] S. Nene, E. Karhu, R.L. Flemming, J.L. Hutter. J. Cryst. Growth. **311**, 4770 (2009).
[18] E. Blázquez-Blázquez, R. Barranco-Garcí—a, M.L. Cerrada, J.C. Martínez, E. Pérez. Polymers **12**, *6*, 1341 (2020).
[19] F. Rajabalee, V. Metivaud, D. Mondieig, Y. Haget, M.A. Cuevas-Diarte. J. Mater. Res. **14**, *6*, 2644 (1999).
[20] K. Nozaki, N. Higashitani, T. Yamamoto, T. Hara. J. Chem. Phys. **103**, *13*, 5762 (1995).
[21] R.G. Snyder, M. Maroncelli, S.P. Qi, H.L. Strauss. Science **214**, *4517*, 188 (1981).
[22] B. Ewen, G.R. Strobl, D. Richter. Faraday Discuss. Chem. Soc., **69**, 19 (1980).
[23] V.M. Egorov, A.K. Borisov, V.A. Marikhin. FTT **63**, *3*, 498 406 (2021).
[24] A.K. Borisov, V.A. Marikhin, V.M. Egorov. FTT **66**, *5*, 726 752 (2024).
[25] S.R. Craig, G.P. Hastie, K.J. Roberts, J.N. Sherwood. J. Mater. Chem. **4**, *6*, 977 (1994).
[26] R.D. Svetogorov, P.V. Dorovatovskii, V.A. Lazarenko. Cryst. Res. Technol. **55**, *5*, 1900184 (2020).
[27] R.D. Svetogorov. Dionis — Diffraction Open Integration Software. Certificate of state registration of computer program № 2018660965, 30.08.2018.
[28] M.A. Poray-Koshitz. Fundamentals of structural analysis of chemical compounds: Ucheb. posobie. M.: Higher School (1989). p. 192. (in Russian).
[29] B.N. Rolov, V.E. Yurkevitch. Fizika razmytykh fazovykh perekhodov. Izd-vo Rostov. un-ta, Rostov (1983). 350 c. (in Russian).
[30] G.A. Malygin. Physics–Uspekhi **44**, 173 (2001).

Translated by A.Akhtyamov